Multi-Higgs-boson production in gluon fusion at 100 TeV

Céline Degrande,* Valentin V. Khoze,† and Olivier Mattelaer‡
Institute for Particle Physics Phenomenology, Department of Physics, Durham University, Durham DH1 3LE, United Kingdom
(Received 2 June 2016; published 28 October 2016)

We carry out a detailed study of multi-Higgs production processes in the gluon fusion channel in the high-energy regime relevant to future circular hadron colliders and in the high-Higgs-multiplicity limit (≥ 20). Our results are based on the computation of the leading polygons—the triangles, boxes, pentagons and hexagons—to the scattering processes, further combined with the subsequent branchings to reach high final-state multiplicities. The factorial growth of the number of diagrams leads to an exponential enhancement of such large-multiplicity cross sections and, ultimately, to the breaking of perturbativity. We find that the characteristic energy and multiplicity scales where these perturbative rates become highly enhanced and grow with increasing energy are within the 100 TeV regime, on the order of 130 Higgses (or more) in the final state. We also show that already for a 50 TeV hadron collider, the perturbative cross sections for 140 bosons are at the picobarn level.

DOI: 10.1103/PhysRevD.94.085031

I. INTRODUCTION

At very high energies, the production of multiple Higgs and electroweak vector bosons becomes kinematically possible. The cross sections for such processes, computed in perturbation theory, become unsuppressed above a certain critical value of final-state multiplicities, and continue to grow with energy eventually violating perturbative unitarity [1–3]. This results in the breakdown of a weakly coupled perturbation theory and a transition into a nonperturbative regime where the intermediate state formed during the collision is characterized by a collective multiboson configuration with large occupation numbers. The critical energies at which the perturbative high-multiplicity rates become large were estimated recently in Refs. [4,5] and were found to be in the 10^2–10^3 TeV range—i.e., nearly in the reach of current and future experiments. The aim of this paper is to further improve and quantify the critical values of energies and multiplicities for multi-Higgs-boson production. We will argue that already for a 50 TeV hadron collider, the rapid growth of perturbative rates in our model can lead to picobarn cross sections for processes with $\gtrsim$140 Higgs bosons.

There is a strong similarity, already noted in Ref. [4], between these novel perturbative unitarity problems at high multiplicities with hundred-TeV energies, and the well-known unitarity problem for simple 2-to-2 scattering processes of massive vector bosons. This has resulted in a powerful and far-reaching conclusion formulated in Ref. [6] that one of three options has to be realized: either (i) there exists a Higgs boson with a mass below ~1 TeV, or (ii) there should be new physics beyond the Standard Model, or finally, (iii) the scattering processes of electroweak gauge bosons become nonperturbative. This threefold way forward for electroweak physics was answered and resolved by the observation of a Higgs boson at 125 GeV. Now, with the high-multiplicity scatterings at 50–100 TeV center-of-mass energies, the perturbative electroweak physics faces a similar crossroads.

To obtain a reliable estimate for multi-Higgs production processes at energies relevant for future circular hadron colliders (FCC), which kinematically allow for very high Higgs multiplicities in the final state, one has to overcome a number of complications. There are two immediate technical problems one encounters already at the leading order in perturbation theory:

(1) The dominant Higgs production is via the gluon fusion process $gg \to n \times h$, and it requires a computation of Feynman diagrams involving one-loop polygons with $2 + k$ edges, where k is the number of the outgoing Higgs lines, for all $k \leq n$. The numbers of the contributing polygon types and of the corresponding kinematic invariants they depend on grow with n and ultimately explode in the high-multiplicity limit $n \gg 1$. This provides for a challenging computation.

(2) The number of Feynman diagrams describing the subsequent tree-level branching processes $h_i^* \to n_i \times h$ from each of the polygon's external lines h_i^* is known to grow factorially with n, and this is reflected in a factorial explosion of perturbative amplitudes, as shown in Refs. [7–10].

Based on these considerations, it was argued in Refs. [4,5] that the standard weakly coupled

*celine.degrande@durham.ac.uk
†valya.khoze@durham.ac.uk
‡o.p.c.mattelaer@durham.ac.uk

 © 2016 American Physical Society

perturbation theory in the electroweak sector of the Standard Model breaks down for multiparticle production of Higgses and massive vector bosons at energy scales as low as $\sim 10^2$–10^3 TeV. The energies where electroweak processes could enter a novel effectively strongly coupled regime, where the ultrahigh-multiplicity production of relatively soft bosons would become unsuppressed and dominate the total rates, may be potentially within the reach of the next generation of colliders.

We will address the two problems listed above in stages: First, we will consider the polygon contributions to the multi-Higgs cross sections by working in the high-energy limit $\sqrt{s} \to \infty$ with a fixed number of Higgses, $k =$ fixed. Then, we will combine these fixed-multiplicity loop-level results in the ultrahigh-energy limit with the subsequent tree-level branchings. Here each intermediate highly energetic Higgs particle h_i^* emitted at the end of the polygon production stage undergoes the tree-level production $h_i^* \to n_i \times h$ into the high-multiplicity n-Higgs final state, $n = \sum_i n_i$. The full amplitude chain for this process is

$$\mathcal{A}_{gg\to n\times h} = \sum_{\text{polygons}} \mathcal{A}^{\text{polygons}}_{gg\to k\times h^*} \sum_{n_1+\cdots+n_k=n} \prod_{i=1}^{k} \mathcal{A}_{h_i^*\to n_i\times h}. \quad (1.1)$$

The $1_i^* \to n_i$ amplitudes[1] appearing as the rightmost factor in (1.1) can be computed very efficiently for all n_i using the classical generating functions technique. For convenience and future reference, we will now present the result for these amplitudes on multi-Higgs mass thresholds.

The computation of polygon contributions to the processes (1.1) combined with the subsequent branchings and the resulting estimate for the multi-Higgs production cross sections, which is the main motivation of this paper, will be addressed in Secs. II–IV.

A. $\mathcal{A}_{h^*\to n\times h}$ from classical solutions

At tree level, all n-point scattering amplitudes for an off-shell field h to produce n Higgs particles, $\mathcal{A}_{1\to n}$, can be obtained from a classical solution of the Euler-Lagrange equations corresponding to the Higgs Lagrangian

$$\mathcal{L}_h = \frac{1}{2}\partial^\mu h \partial_\mu h - \frac{\lambda}{4}(h^2 - v^2)^2, \quad (1.2)$$

following the generating functions technique initiated in Ref. [7] (where λ is the Higgs self-coupling and v is the vacuum expectation value). For an overview of the classical generating functions technique and its applications, the interested reader can consult the Appendix. In the rest of the current section, we will simply state the features of this approach which are relevant for our study.

As the final state is made out of the outgoing particles, the relevant solution $h_{\text{cl}}(x)$ should contain only the positive-frequency modes, $e^{+\text{in}M_h t}$, where $M_h = \sqrt{2\lambda}v$ is the Higgs boson mass. This specifies the initial conditions, or equivalently the analytic structure of the solution—its time dependence is described by the complex variable z,

$$z(t) = z_0 e^{iM_h t}, \quad (1.3)$$

on which the configuration h_{cl} depends holomorphically:

$$h_{\text{cl}}(\vec{x}, t) = v + \sum_{n=1}^{\infty} a_n(\vec{x}) z(t)^n. \quad (1.4)$$

As there is no dependence on the complex conjugate variable z^*, the required solution is complex (even though the original scalar field h was real) and will also contain singularities in the Euclidean space-time.

We now consider the simplest kinematics, where all the final-state particles are produced at their mass threshold (i.e. with vanishing spacial momenta). In this case, the classical solution in question, h_{cl}, is uniform in space and solves the ordinary differential equation

$$d_t^2 h = -\lambda h^3 + \lambda v^2 h, \quad (1.5)$$

with the initial conditions $h_{\text{cl}} = v + z + \mathcal{O}(z^2)$. This solution is known in closed form [7]:

$$h_{\text{cl}}(t) = v \frac{1 + \frac{z(t)}{2v}}{1 - \frac{z(t)}{2v}}. \quad (1.6)$$

This is the exact solution of the classical equation (1.5), as can be readily checked, for example, in Mathematica. In the Appendix we also explain how to derive this expression analytically.

We note that (in real time) this expression is complex and that it is singular on the complex time plane at $z = 2v$. The singularity of the solution is the consequence of the finite radius of convergence of the Taylor expansion of (1.6),

$$h_{\text{cl}}(t) = v + 2v \sum_{n=1}^{\infty} \left(\frac{z(t)}{2v}\right)^n. \quad (1.7)$$

The classical solution h_{cl} defines the generating functional for the tree-level scattering amplitudes. All n-point tree-level amplitudes at threshold are simply given by differentiating n times with respect to z [7],

$$\mathcal{A}_{1\to n} = \left(\frac{\partial}{\partial z}\right)^n h_{\text{cl}}\Big|_{z=0} = n!(2v)^{1-n}, \quad (1.8)$$

and they exhibit factorial growth with the number of particles in the final state. Equations (1.6) and (1.8), describing the tree-level amplitudes on the multiparticle mass thresholds,

[1] We will always adopt the shorthand convention that the propagator for the incoming virtual Higgs was not LSZ amputated, i.e. $\mathcal{A}_{h_i^*\to n_i\times h} := \frac{1}{s_i - M_h^2}\mathcal{A}^{\text{LHZ}}_{h_i^*\to n_i\times h}$.

will play an important role in our approach in the main part of this paper.[2]

Such threshold amplitudes were further generalized to other scalar field theories and also computed at the one-loop and resummed multi-loop levels in Refs. [11–16]. The multiparticle amplitudes on threshold were also computed in the gauge Higgs theory in Ref. [10], confirming their factorial growth in reference to probing the electroweak sector at high FCC energies [4,5].

For general kinematics, with momenta above the multiparticle mass threshold, the scattering amplitudes $\mathcal{A}_{1\to n}$ at tree level are still given by the classical solution $h_{\rm cl}(\vec{x},t)$ of equations of motion—they are no longer uniform in space, having instead the $O(3)$ spherical symmetry. These solutions are uniquely specified by the same initial conditions as $z\to 0$, and are singular on hypersurfaces in the Euclidean space-time. They could be found numerically by searching for classical extrema of the path integral on the appropriate singular complex-valued field configurations as explained in Refs. [17–20]. This is a complicated procedure, and the closed-form expressions for such $O(3)$ symmetric solutions are presently unknown even in the simplest scalar QFT models.

Alternatively, one can derive the amplitudes' and cross sections' dependence on the external state's kinematics at tree level by solving the full $(3+1)$-dimensional Euler-Lagrange equations recursively in n. This is achieved by writing down the perturbative recursion relations corresponding to the classical solutions, as explained in Refs. [9,21,22], and solving them first in the nonrelativistic limit, and then in general kinematics. The latter step is required to enable the integration over the n-particle phase space to obtain the cross-section. This program was carried out in Ref. [5] using Madgraph5_aMC@NLO [23,24]. The approach followed in this paper will not require the knowledge of the $\vec{x}$-dependent singular solutions; instead, we will use the formalism and results of Ref. [5] based on combining the known scaling behavior at large n inferred from the mass-threshold amplitude (1.8), with a numerical computation of tree-level cross sections at fixed n directly.

This paper is organized as follows: In Sec. II, we will compute the gluon fusion cross sections for the double, triple, and quadruple Higgs production at fixed center-of-mass gluon energies in the range between 10 and 160 TeV. We will identify the contributions coming from the triangles, boxes, pentagons and hexagons, and represent them in the high-energy regime in terms of effective vertices with energy-dependent form factors. We will demonstrate that this approximation is well justified in the high-energy kinematics where $\sqrt{s}$ is much greater than the masses of the Higgs and the top quark. We will then combine the effective vertices with the classical generating functions for tree-level amplitudes describing the subsequent multi-Higgs branchings. In this way, we will obtain the generating functions for scattering amplitudes describing $gg\to n\times h$ processes in the high-multiplicity regime near the multiparticle mass thresholds. We will use these results in Sec. III to estimate the multiparticle cross sections based on their scaling behavior with multiplicity and energy [5,9]. Finally, in Sec. IV, we will convolute the partonic cross sections with the parton distribution functions (PDFs) of the gluons. Our projections for the high-multiplicity Higgs production cross sections at proton-proton colliders are summarized in Fig. 6, and our conclusions are presented in Sec. V.

II. POLYGONS AND EFFECTIVE VERTICES IN THE $\sqrt{s}\to\infty$ LIMIT

We now consider the first stage of the process (1.1) involving the high-energy fixed-multiplicity k-Higgs production $\mathcal{A}^{\rm polygons}_{gg\to k\times h^*}$. The double and triple Higgs production at colliders was studied in Refs. [25–28] and [29–32] and is rather suppressed at the LHC and the FCC energies. Our main goal, however, is to determine whether the *high-multiplicity* rates with $n\gg 2,3$ Higgses can become unsuppressed in perturbation theory. As explained in the Introduction, we will address the large-n limit by computing the fixed-multiplicity $gg\to k\times h^*$ one-loop processes in the high-energy limit and combining them with the subsequent $h^*\to n_i\times h$ branchings, cf. Eq. (1.1).

Using the Madgraph5_aMC@NLO framework [33], we computed the double, triple and quadruple Higgs production cross sections in the gluon fusion channel at one-loop level in the high-energy regime. Specifically, with the applications to the FCC hadronic colliders in mind, we concentrate on the center-of-mass energies $\sqrt{s}$ much greater than the Higgs and top quark masses.

The first panel in Fig. 1 shows our results for the Higgs pair production and the triple Higgs production, and the second panel gives the cross sections for the quadruple Higgs. The contributions from each type of polygon are shown separately (and we do not compute the interference terms between different polygon types). For example, the *triangles* category corresponds to the sum of all Feynman diagrams containing the $gg\to h^*$ one-loop triangles contributing to the $gg\to h^*\to n\times h$ amplitude for $n=2,3,4$. The resulting amplitude is squared and integrated over the phase space to obtain the cross-section contributions induced by the triangles. The process is then repeated for higher polygons: boxes, pentagons and hexagons.[3]

The interference terms between polygons with different numbers of sides (e.g. interferences between the triangle-induced and the box-induced contributions to the cross

[2]These are exact results for the tree-level n-point amplitudes on mass thresholds for arbitrary values of n.

[3]To be clear, in our notation the polygon ranks (i.e. the number of polygon edges) is $2+k$, where $1\le k\le n$, so that e.g. pentagons ($k=3$) contribute to $gg\to 3\times h^*\to n\times h$ processes with $n=3,4,\ldots$

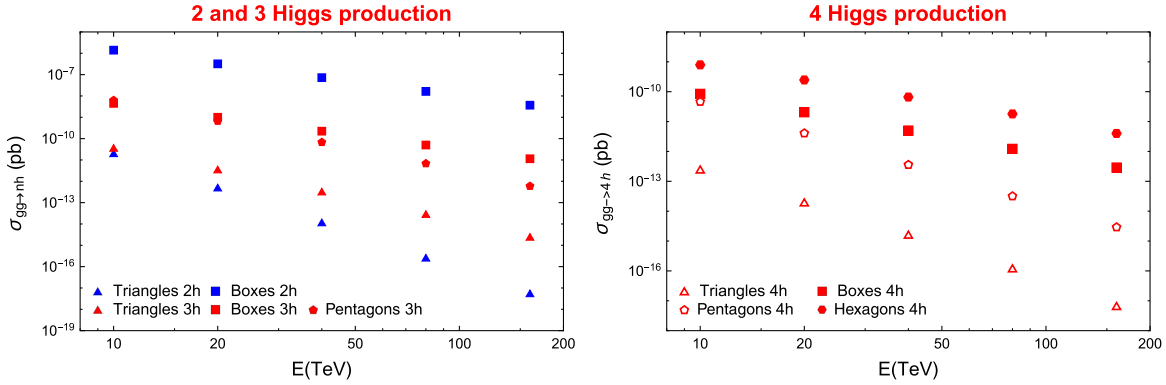

FIG. 1. Cross sections for two-Higgs, three-Higgs and four-Higgs production in the gluon fusion process separated into contributions from triangles, boxes, pentagons and hexagons, as indicated. Gluons are scattered at fixed energy (i.e., no gluon PDFs included) in order to simplify the s dependence of these cross sections at the partonic level.

sections) are not accounted for in the computation presented in Fig. 1. However, based on the fact that different polygon types give a very clear numerical hierarchy of the cross-sectional values, as seen from Fig. 1 (and similarly have different analytic dependences on the parameters, as will be seen in Tables I and II below), we expect that the missing interference terms will not modify our results dramatically.

By varying the Higgs and top masses as well as the center-of-mass energy $\sqrt{s}$, we can extract from these data the analytic scaling properties for different polygonal contributions to the cross sections applicable in the high-energy regime. These scaling properties are summarized in Table I. The polygons with different numbers of edges are treated separately, so that the different entries in the table do not mix (e.g. triangles with boxes); each horizontal entry is specific to a particular type of polygon as indicated and contains no cross terms between polygons with different numbers of edges. We have also fixed the energy of the gluon (i.e., we are considering partonic cross sections with no gluon PDFs) in order to focus on the s dependence of the cross sections at the partonic level.[4] It follows that all even polygons (boxes, hexagons, etc.) exhibit the same $1/s$ scaling in the high-energy limit $\sqrt{s} \gg M_h, m_t$. At the same time, the odd polygons (triangles, pentagons, and so on) are subdominant and go as $1/s^2 \log^4(m_t/\sqrt{s})$ (with the exception of the leading double-Higgs case, where the suppression is even stronger).

The high-energy behavior of the leading-rank polygons in Table I can now be easily generalized to higher multiplicities and higher polygon ranks following the same pattern. For polygons with $2+k$ edges, their contribution to the $gg \to n \times h$ process is

$$(2+k)\text{−polygons: } \sigma_{gg\to n\times h} \propto \frac{1}{s} y_t^{2k} \left(\frac{M_h}{v}\right)^{2(n-k)} \times \begin{cases} 1 & : k = \text{even} \\ \frac{m_t^2}{s} \log^4\left(\frac{m_t}{\sqrt{s}}\right) & : k = \text{odd}. \end{cases} \tag{2.1}$$

The only exception from this rule is the $k=1$, $n=2$ case; i.e., the leftmost triangle in Table I, which has an additional factor of M_h^2/s. As a matter of fact, the squared amplitude in multi-Higgs production with a odd number of three Higgs vertices is enhanced compared to a naive counting by

TABLE I. High-energy scaling behavior of each polygon type's contributions to the gluon fusion multi-Higgs production cross sections, extracted from numerical data as in Fig. 1, and shown as a function of s, M_h and m_t and $y_t := \sqrt{2} m_t/v$ in the $s \gg m_t, M_h$ limit. All cross sections also contain the common factor of $\alpha_s^2(\sqrt{s})$. Gluon PDFs are not included.

	$\sigma_{gg\to hh}$	$\sigma_{gg\to hhh}$	$\sigma_{gg\to hhhh}$
Triangles	$y_t^2 \frac{m_t^2 M_h^2}{s^3} \log^4\left(\frac{m_t}{\sqrt{s}}\right) \frac{M_h^2}{v^2}$	$y_t^2 \frac{m_t^2}{s^2} \log^4\left(\frac{m_t}{\sqrt{s}}\right) \frac{M_h^4}{v^4}$	$y_t^2 \frac{m_t^2}{s^2} \log^4\left(\frac{m_t}{\sqrt{s}}\right) \frac{M_h^6}{v^6}$
Boxes	$y_t^4 \frac{1}{s}$	$y_t^4 \frac{1}{s} \frac{M_h^2}{v^2}$	$y_t^4 \frac{1}{s} \frac{M_h^4}{v^4}$
Pentagons	$\cdots$	$y_t^6 \frac{m_t^2}{s^2} \log^4\left(\frac{m_t}{\sqrt{s}}\right)$	$y_t^6 \frac{m_t^2}{s^2} \log^4\left(\frac{m_t}{\sqrt{s}}\right) \frac{M_h^2}{v^2}$
Hexagons	$\cdots$	$\cdots$	$y_t^8 \frac{1}{s}$

TABLE II. High-energy scaling behavior for multi-Higgs production cross sections with the bare effective vertices [Eq. (2.2)] obtained with FeynRules [34] and Madgraph5_aMC@NLO.

	$\sigma^{\text{eft}}_{gg\to hh}$	$\sigma^{\text{eft}}_{gg\to hhh}$	$\sigma^{\text{eft}}_{gg\to hhhh}$
$\alpha_s \text{tr}(G_{\mu\nu} G^{\mu\nu}) h^1$	$\frac{M_h^2}{v^2} s^0$	$\frac{M_h^4}{v^4} s^0$	$\frac{M_h^6}{v^6} s^0$
$\alpha_s \text{tr}(G_{\mu\nu} G^{\mu\nu}) h^2$	s	$\frac{M_h^2}{v^2} s$	$\frac{M_h^4}{v^4} s$
$\alpha_s \text{tr}(G_{\mu\nu} G^{\mu\nu}) h^3$	$\cdots$	s^2	$\frac{M_h^2}{v^2} s^2$
$\alpha_s \text{tr}(G_{\mu\nu} G^{\mu\nu}) h^4$	$\cdots$	$\cdots$	s^3

[4]The proton-proton collisions and the convolution of the partonic cross sections with gluon PDFs will be discussed in Sec. IV.

TABLE III. Operator coefficients in Eq. (2.3). Each C_k appears to be largely independent of the number of Higgses in the full matching process $gg \to n \times h$ and describes the rates well at all energies in the high-energy range $\sqrt{s} \gg M_h, m_t$.

C_2	$\sqrt{s} = 10$ TeV	$\sqrt{s} = 20$ TeV	$\sqrt{s} = 40$ TeV	$\sqrt{s} = 80$ TeV	$\sqrt{s} = 160$ TeV
$gg \to hh$	1.12	1.13	1.14	1.14	1.14
$gg \to hhh$	1.11	1.13	1.14	1.14	1.14
$gg \to hhhh$	1.21	1.23	1.23	1.23	1.21
C_3	$\sqrt{s} = 10$ TeV	$\sqrt{s} = 20$ TeV	$\sqrt{s} = 40$ TeV	$\sqrt{s} = 80$ TeV	$\sqrt{s} = 160$ TeV
$gg \to hhh$	7.91	7.95	8.16	8.59	8.60
$gg \to hhhh$	8.52	8.42	8.43	8.68	8.86
C_4	$\sqrt{s} = 10$ TeV	$\sqrt{s} = 20$ TeV	$\sqrt{s} = 40$ TeV	$\sqrt{s} = 80$ TeV	$\sqrt{s} = 160$ TeV
$gg \to hhhh$	4.34	5.10	5.55	6.11	6.04

a factor s/M_h^2 when the invariant mass appearing in the propagator is close to its minimal value of order M_h. In the case of pair production, the only invariant mass is fixed at $\sqrt{s}$, and therefore such enhancement is absent.

The pattern established in Table I and Eq. (2.1) enables us to simplify the full one-loop Feynman diagram–based computation in Fig. 1 by reducing it to contributions from effective multi-Higgs vertices of the form

$$V_k^{\text{eft}} \sim \alpha_s \text{tr}(G_{\mu\nu} G^{\mu\nu}) h^k, \tag{2.2}$$

where $\sim$ indicates that the dimension-$(4+k)$ operators on the right-hand side should be multiplied by the appropriate energy-dependent form factors $F_k(s)$. These form factors will be determined momentarily.

To proceed, we first consider the contributions to cross sections from the bare effective operators (2.2); i.e., not including the form factors. The corresponding cross sections are found to grow with s, as summarized in Table II, and this is of course also consistent with a simple dimensional analysis in the high-energy limit. The form factors $F_k(\sqrt{s})$ can now be determined by matching the contributions from $\mathcal{V}_k \coloneqq V_k^{\text{eft}} \times F_k(\sqrt{s})$ of Table II to Table I. We find the following expressions for the effective vertices (including the form factors):

$$\mathcal{V}_k = C_k \frac{\alpha_s(\sqrt{s})}{\pi} \text{tr}(G_{\mu\nu} G^{\mu\nu}) \left(\frac{y_t h}{\sqrt{s}}\right)^k \times \begin{cases} 1 & : k = \text{even} \geq 2 \\ \dfrac{m_t}{\sqrt{s}} \log^2\left(\dfrac{m_t}{\sqrt{s}}\right) & : k = \text{odd} \geq 3. \end{cases} \tag{2.3}$$

Here, C_k's are the constant coefficients to be determined by matching to the full numerical cross section results, and y_t is the top quark Yukawa coupling.

The coefficients C_k can now be found by matching the cross sections σ^{eft} computed from the effective field theory (EFT) vertices (2.3) to our numerical results for the complete partonic cross sections shown in Fig. 1. Specifically, the two-point effective vertices are matched to boxes, the three-point EFTs are matched to pentagons, and the four-point vertices are matched to the hexagon-induced contributions to the cross sections. For each effective vertex of rank k, the coefficient C_k can be obtained in $n-k$ independent ways from matching:

$$C_2 : \sigma_{gg\to n\times h}[\mathcal{V}_2] \leftrightarrow \sigma_{gg\to n\times h}[\text{Boxes}], \quad \text{for } n = 2,3,4,\ldots \tag{2.4}$$

$$C_3 : \sigma_{gg\to n\times h}[\mathcal{V}_3] \longleftrightarrow \sigma_{gg\to n\times h}[\text{Pentagons}], \quad \text{for } n = 3,4,\ldots \tag{2.5}$$

$$C_4 : \sigma_{gg\to n\times h}[\mathcal{V}_4] \longleftrightarrow \sigma_{gg\to n\times h}[\text{Hexagons}], \quad \text{for } n = 4,\ldots \tag{2.6}$$

and for different values of the center-of-mass energy $\sqrt{s}$. Their values are shown in Table III. We conclude that the extracted numerical values of these coefficients do not appear to depend strongly on the number of Higgses in the final state. This is an important test for our approach; it guarantees the robustness of the effective vertices approximation (2.3) for the multi-Higgs production cross sections in the high-energy limit.

Our construction up to this point was derived from taking the high-energy limit and holding the Higgs multiplicity fixed. The next step is to use the effective vertices (2.3) combined with the classical generating functionals for the tree-level amplitudes introduced in Sec. I A to address the desired high-multiplicity limit $n \gg 1$. This is achieved by substituting the Higgs fields h in the effective vertices with the generating functionals for $1^* \to n$ scattering amplitudes $\mathcal{A}_{h^*\to n\times h}$.

The resulting generating functionals for the two gluons into any number of Higgs processes are given by the effective vertices $\mathcal{V}_k$ in Eq. (2.3) with the substitutions $h^k \to h_{\text{cl}}[z]^k$ and $\text{tr}(G_{\mu\nu}G^{\mu\nu}) \to (p_{1\mu}\epsilon_{1\nu}^a - p_{1\nu}\epsilon_{1\mu}^a)(p_2^\mu \epsilon_2^{a\nu} - p_2^\nu \epsilon_2^{a\mu})$.

Here p_1, p_2 are the gluon momenta and ϵ_1^a, ϵ_2^b are their helicities, while $h_{\rm cl}[z]$ is the generating functional (1.4).

Using the classical solution (1.6) (shifted by the vacuum expectation value) $h_{\rm cl} \to h_{\rm cl} - v$, we can immediately write down the generating functional of multi-Higgs amplitudes on the multiparticle mass threshold in closed form:

$$\mathcal{A}^{k=\text{even}}[z] = C_k \frac{\alpha_s}{\pi}(p_{1\mu}\epsilon_{1\nu}^a - p_{1\nu}\epsilon_{1\mu}^a)(p_2^\mu \epsilon_2^{a\nu} - p_2^\nu \epsilon_2^{a\mu}) \times \left(\frac{y_t}{\sqrt{s}}\frac{z}{1-\frac{z}{2v}}\right)^k. \tag{2.7}$$

Here we took the polygon/EFT vertex rank k to be even valued, since for odd k the effective vertices in (2.3) are suppressed by the factor $\frac{m_t}{\sqrt{s}}\log^2(\frac{m_t}{\sqrt{s}}) \ll 1$.

The high-multiplicity regime of interest for us is

$$\sqrt{s} \gg \text{all other mass scales}, \quad \text{and} \quad n \gg 1, \tag{2.8}$$

and it will also be convenient to define the average final-state kinetic energy per particle per mass, ε, via

$$\varepsilon := \frac{\sqrt{s} - nM_h}{nM_h}. \tag{2.9}$$

On the multiparticle mass threshold $\varepsilon = 0$, but more generally above the threshold, we will work in the limit where ε is held fixed at some nonvanishing value[5] as $\sqrt{s}$ and n become $\gg 1$.

The n-Higgs amplitudes on the multiparticle mass thresholds read [cf. (1.8)]

$$\begin{aligned}\mathcal{A}^{k\,\text{thr.}}_{gg\to n\times h} &= C_k \frac{\alpha_s}{\pi}(p_{1\mu}\epsilon_{1\nu}^a - p_{1\nu}\epsilon_{1\mu}^a)(p_2^\mu \epsilon_2^{a\nu} - p_2^\nu \epsilon_2^{a\mu}) \times \left(\frac{\partial}{\partial z}\right)^n \left(\frac{y_t}{\sqrt{s}}\frac{z}{1-\frac{z}{2v}}\right)^k\Bigg|_{z=0} \\ &\sim C_k \frac{\alpha_s}{\pi} y_t^k \left(\frac{1}{1+\varepsilon}\right)^{k-2}\left(\frac{1}{nM_h}\right)^{k-2} \times \left(\frac{\partial}{\partial z}\right)^n \left(\frac{z}{1-\frac{z}{2v}}\right)^k\Bigg|_{z=0},\end{aligned} \tag{2.10}$$

where in the final expression we use the substitutions $(p_1+p_2)^2 = s$ and $\sqrt{s} = (1+\varepsilon)nM_h$. Of course, the true threshold amplitude is obtained from (2.10) by setting $\varepsilon = 0$.

We now note that since

$$\left(\frac{\partial}{\partial z}\right)^n h_{\rm cl}[z]\Big|_{z=0} = \left(\frac{\partial}{\partial z}\right)^n \left(\frac{z}{1-\frac{z}{2v}}\right)\Bigg|_{z=0} = n!\left(\frac{1}{2v}\right)^{n-1}, \tag{2.11}$$

the same operation applied to the kth power of the classical solution will lead in the large-n limit to

$$\left(\frac{\partial}{\partial z}\right)^n \left(\frac{z}{1-\frac{z}{2v}}\right)^k\Bigg|_{z=0} \to n^{k-1}n!\left(\frac{1}{2v}\right)^{n-k-1}. \tag{2.12}$$

In particular, it can be verified that for $k = 2$ (boxes), the expression valid for all values of n is

$$\left(\frac{\partial}{\partial z}\right)^n \left(\frac{z}{1-\frac{z}{2v}}\right)^2\Bigg|_{z=0} = (n-1)n!\left(\frac{1}{2v}\right)^{n-3}, \tag{2.13}$$

and for $k = 4$ (hexagons), one gets

$$\left(\frac{\partial}{\partial z}\right)^n \left(\frac{z}{1-\frac{z}{2v}}\right)^4\Bigg|_{z=0} = \frac{1}{6}(n^3 - 6n^2 + 11n - 6)n!\left(\frac{1}{2v}\right)^{n-5}. \tag{2.14}$$

To summarize, the threshold amplitudes ($\epsilon = 0$) in the large-n limit read

$$\mathcal{A}^{k\,\text{thr.}}_{gg\to n\times h}\big|_{\epsilon=0} \to nn!\left(\frac{\lambda}{2M_h^2}\right)^{\frac{n-1}{2}} \frac{C_k}{\kappa_k}\frac{\alpha_s}{\pi} M_h^2 \left(\frac{2m_t}{M_h}\right)^k, \tag{2.15}$$

where $\kappa_2 = 1$ and $\kappa_4 = 6$. Above the threshold, we should also include the multiplicative factor $1/(1+\varepsilon)^{k-2}$ present on the right-hand side of (2.10). Hence, one can write for the above-the-threshold amplitude

$$\mathcal{A}^k_{gg\to n\times h} = n\left(\frac{1}{1+\varepsilon}\right)^{k-2} \frac{C_k}{\kappa_k}\frac{\alpha_s}{\pi} M_h^2 \left(\frac{2m_t}{M_h}\right)^k \mathcal{A}_{h^*\to n\times h}, \tag{2.16}$$

and in addition, one should remember that the tree-level amplitude on the right-hand side will itself contain dependence on the kinematics. For example, in the double-scaling large-n $\varepsilon \ll 1$ limit with $n\varepsilon$ held fixed, the tree-level amplitudes in the Higgs model were computed in Ref. [22]:

$$\mathcal{A}_{h^*\to n\times h} = n!\left(\frac{\lambda}{2M_h^2}\right)^{\frac{n-1}{2}} \exp\left[-\frac{7}{6}n\varepsilon\right]. \tag{2.17}$$

We will postpone the discussion of the full kinematic dependence for these processes to the next section.

The main conclusions we would like to draw from the discussion up to now is that in the high-energy, large-n limit, the dominant contributions to the multiparticle amplitudes are succinctly characterized by the set of EFT vertices (2.3) or generating functionals (2.10) with even values of $k \geq 2$. Further simplification occurs in the highly relativistic kinematics where ε is large. In this case, the factor $1/(1+\varepsilon)^{k-2} \ll 1$ in (2.16) suppresses all contributions from $k > 2$—hence, in this case the dominant contributions come from the boxes.

In the kinematic regime where $\varepsilon \lesssim 1$, all even-k polygons contribute and are described by the amplitudes (2.15). The

[5]Corresponding to either a nonrelativistic ($\varepsilon < 1$) or a highly relativistic ($\varepsilon > 1$) regime.

constants C_2 and C_4 were computed in Table III together with $\kappa_2 = 1$ and $\kappa_4 = 6$. Hence, the numerical prefactors for the boxes and the hexagons are fully accounted for. But the main point of our analysis is that all even polygons contribute to the same n dependence of the amplitudes in (2.15), and the cross sections at large n will have the characteristic same exponential behavior which will be determined in the following section.

III. EXPONENTIAL FORM OF THE MULTIPARTICLE CROSS SECTION

Let us consider the multiparticle limit $n \gg k \approx 1$ and scale the energy $\sqrt{s} = E$ linearly with n, $E \propto n$, keeping the coupling constant small at the same time, $\lambda \propto 1/n$. Based on the characteristic form $\sim n!\lambda^{n/2}$ of the multiparticle scattering amplitudes on and above the multiparticle thresholds, it was first pointed out in Ref. [9], and then argued for extensively in the literature, that in this double-scaling limit the production cross sections σ_n have a characteristic exponential form,

$$\sigma_n \sim e^{nF(\lambda n,\varepsilon)}, \quad \text{for } n \to \infty, \qquad \lambda n = \text{fixed}, \quad \varepsilon = \text{fixed}, \tag{3.1}$$

where ε is the average kinetic energy per particle per mass in the final state (2.9), and $F(\lambda n, \varepsilon)$ is a certain *a priori* unknown function of two arguments, often referred to as the "holy grail" function for the multiparticle production. At tree-level, the dependence on λn and ε factorizes into individual functions of each argument,

$$F^{\text{tree}}(\lambda n, \varepsilon) = f_0(\lambda n) + f(\varepsilon), \tag{3.2}$$

and the two independent functions are given by the following expressions in the Higgs model (1.2) (see Refs. [9,22]):

$$f_0(\lambda n) = \log\left(\frac{\lambda n}{4}\right) - 1, \tag{3.3}$$

$$f(\varepsilon)|_{\varepsilon\to 0} \to f(\varepsilon)_{\text{asympt}} = \frac{3}{2}\left(\log\left(\frac{\varepsilon}{3\pi}\right) + 1\right) - \frac{25}{12}\varepsilon. \tag{3.4}$$

These formulas are the result of integrating the tree-level amplitude expressions (2.17) over the Lorentz-invariant phase space, $\sigma_n = \frac{1}{n!}\int \Phi_n |\mathcal{A}_n|^2$, in the large-$n$ nonrelativistic approximation. In particular, the ubiquitous factorial growth of the large-n amplitudes (2.17) translates into the $\frac{1}{n!}|\mathcal{A}_n|^2 \sim n!\lambda^n \sim e^{n\log(\lambda n)}$ factor in the cross section, which determines the function $f_0(\lambda n)$ in (3.3). The energy dependence of the cross section is dictated by $f(\varepsilon)$ in Eq. (3.1), and this function arises from integrating the ε-dependent factors in (2.17) over the phase space, giving rise to the small-ε asymptotics in (3.4). While the function $f_0(\lambda n)$ is fully determined at tree level, the second function, $f(\varepsilon)$, characterizing the energy dependence of the final state, is determined by (3.4) only at small ε—i.e., near the multiparticle threshold.

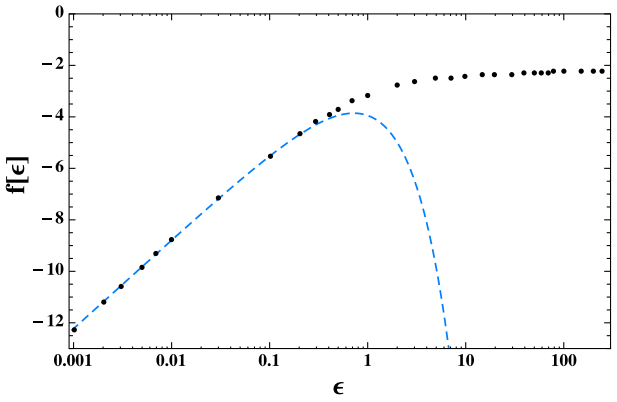

FIG. 2. Plot of $f(\varepsilon)$ extracted from the $\log \sigma_7^{\text{tree}}/\sigma_6^{\text{tree}}$ Madgraph data in Ref. [5]. The results perfectly match $f(\varepsilon)_{\text{asympt}}$ for $\varepsilon < 1$, shown as the dashed curve. In the UV regime, the function asymptotes to a constant $f(\varepsilon = 250) \simeq -2.2$.

The function $f(\varepsilon)$ in the *entire range* of $0 \le \varepsilon < \infty$ was obtained in Ref. [5] from the direct computation of tree-level perturbative cross sections with up to $n = 7$ Higgs particles, combined with the known large-n scaling of the cross section as defined by $f_0(\lambda n)$ in Eqs. (3.2)–(3.3). The function $f_0(\varepsilon)$ is shown in Fig. 2. This plot also shows a perfect match to the known $f(\varepsilon)_{\text{asympt}}$ expression (3.4) at $\varepsilon < 1$, which is shown as a dashed curve in light blue.

Having determined the n-independent kinetic energy function $f(\varepsilon)$ allows to us to compute multiparticle cross sections at any n in the large-n limit.

Let us now consider the effect of higher loop corrections in a single tree process[6] $h^\star \to n \times h$. It was shown in Ref. [9], based on the analysis of leading singularities of the multiloop expansion around singular generating functions in scalar field theory, that the one-loop correction exponentiates and results in the modified expression for f_0,

$$f_0(\lambda n)^{\text{NLO-resummed}} = \log\left(\frac{\lambda n}{4}\right) - 1 + \sqrt{3}\frac{\lambda n}{4\pi}. \tag{3.5}$$

Finally, we can now use the expression for the EFT vertex (2.15) and represent the cross section via

$$\sigma_n = K_k \frac{n^2}{s}\left(\frac{1}{1+\varepsilon}\right)^{2(k-2)} e^{n(f_0(\lambda n)+f(\varepsilon))} = K_k \frac{1}{M_h^2}\left(\frac{1}{1+\varepsilon}\right)^{2k-2} e^{n(f_0(\lambda n)+f(\varepsilon))}. \tag{3.6}$$

In the above formula, all even values of $k \ge 2$ can contribute. We think of k as a characteristic k value for which the prefactor, denoted as K_k in (3.6), would be

[6]Therefore including only the factorable loop for a process with $k > 1$.

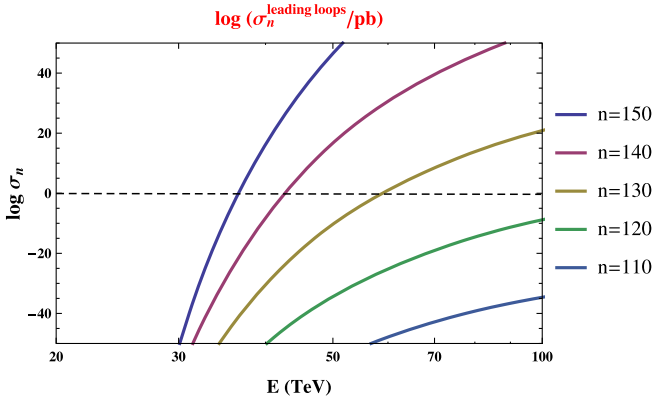

FIG. 3. The logarithm of the cross section (3.8) (in picobarns) is plotted as the function of energy for a range of final-state multiplicities between $n = 110$ and $n = 150$. We used the one-loop improved expression (3.5) for $f_0(\lambda n)$. The plot corresponds to $k = 2$ (boxes), but there are only slight visible differences from the higher case $k = 4$ (hexagons) cf. Fig. 4.

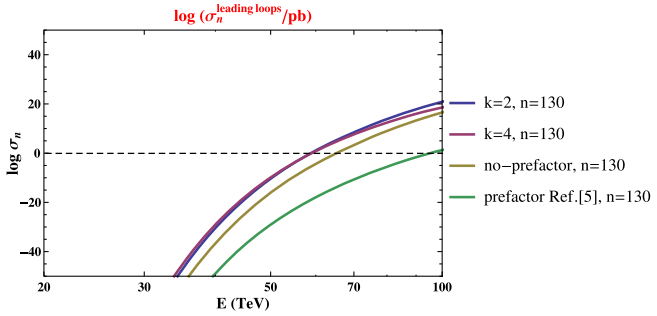

FIG. 4. The logarithm of the n-particle cross section (3.8) for $n = 130$, shown as the function of energy. The four contours represent four different choices for the prefactor: the first two correspond to the $k = 2$ and $k = 4$ expressions in (3.8), and the third contour contains no prefactor, while the fourth case depicts the triangle EFT form factor used in Eqs. (3.12)–(3.13) of Ref. [5].

maximal. This prefactor contains numerical factors appearing in the squared amplitude (2.15):

$$K_k \sim \left(\frac{C_k \alpha_s}{\kappa_k \pi}\right)^2 \left(\frac{2\sqrt{2} m_t}{M_h}\right)^{2k} \simeq \begin{cases} 0.1 & : k = 2 \\ 20 & : k = 4. \end{cases} \tag{3.7}$$

For a practical calculation, we can take $k = 2$ and $k = 4$ and plot the logarithm of the cross section (3.6) for these two cases using the formulas

$$\log(\sigma_n/\text{pb}) \simeq \begin{cases} n(f_0(\lambda n) + f(\varepsilon)) - 2\log(1+\varepsilon) + 8 & : k = 2 \\ n(f_0(\lambda n) + f(\varepsilon)) - 6\log(1+\varepsilon) + 13 & : k = 4. \end{cases} \tag{3.8}$$

The plot in Fig. 3 plots these cross sections as the function of energy for a range of final-state Higgs multiplicities between $n = 110$ and $n = 150$. The specific form of the prefactor for $k = 2$ and $k = 4$ has an almost negligible effect on the logarithm of the cross sections, and the plot depicts only the minimal $k = 2$ case. In Fig. 4, we choose a "relatively low" final-state Higgs multiplicity of $n = 130$ and show the limits derived in the earlier work [5] (based on using the dimension-5 EFT vertices with form factors)[7] versus the cross-section expressions obtained with prefactors based on boxes ($k = 2$), hexagons ($k = 4$), and with no prefactors. We conclude that there is little difference in practice between the latter three cases, while they all show improvement relative to the dimension-5 EFT vertices.

The fact that the leading-loop correction to the tree-level amplitudes on multiparticle mass thresholds exponentiate and result in Eq. (3.5) is a well-established fact [9,16,21] based on a complete multiloop computation in the background of the classical solution (1.6) at its singular point. The fact that loop correction [the last term in (3.5)] is positive in the Higgs theory (1.2) is instrumental in lowering the energy scale where the cross sections stop being small to $\mathcal{O}(100\ \text{TeV})$ and $n \sim 130$. If one wished to use the pure tree-level expression for $f_0(\lambda n)$ in Eq. (3.3), both the desired energy scale and the multiplicity will increase by an order of magnitude, as can be seen from Fig. 5 of Ref. [5].

Of course, one should keep in mind that there are even higher order corrections to the exponent of the multiparticle cross sections arising from the higher loop effects. Moreover, only the loop inside the trees is included and not those connecting different trees. Hence, the use of the one-loop improved expression in (3.5) should be seen as an optimistic phenomenological model. In general, the higher-order effects of loop exponentiation will amount to

$$f_0(\lambda n)^{\text{all loops}} = \log\left(\frac{\lambda n}{4}\right) - 1 + \sqrt{3}\frac{\lambda n}{4\pi} + \text{const}\left(\frac{\lambda n}{4\pi}\right)^2 + \text{const}'\left(\frac{\lambda n}{4\pi}\right)^3 + \ldots \tag{3.9}$$

and can change the cross sections' contours in Fig. 3.[8] Furthermore, the exponentiation of loop-level effects which was proven for amplitudes on mass thresholds is not the full story; one expects that there are additional multiloop contributions to the holy grail function $F(\lambda n, \varepsilon)$, which depend on both λn and ε and cannot be separated into $f_0(\lambda n)$ and $f(\varepsilon)$.

However, what we can state with certainty is that the perturbation theory becomes strongly coupled and breaks down for multiparticle processes when amounts on the

[7]The choice $n = 130$ is motivated by being on the very edge of potential observability, $\log \sigma_n \to 1$, at 100 TeV in the setup of Ref. [5].

[8]Note that the loop expansion parameter $\frac{\lambda n}{4\pi}$ is $\simeq 1$ for $n = 100$ and $\simeq 1.4$ for $n = 140$.

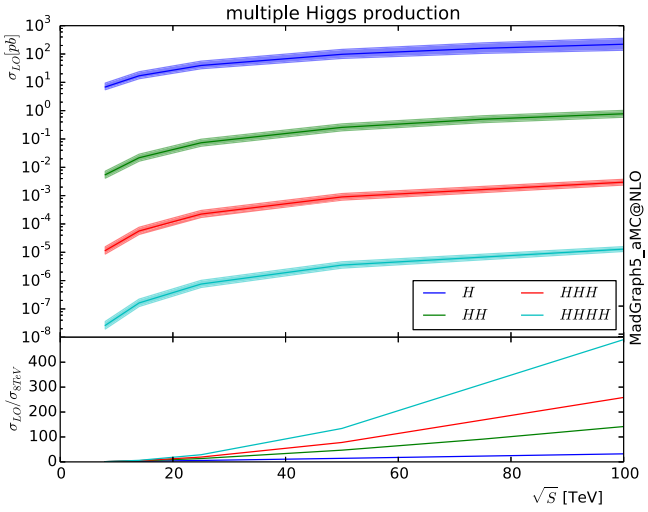

FIG. 5. Leading-order cross sections with up to four Higgs bosons, computed by Madgraph5_aMC@NLO using MSTW2008 PDF [35]. The bands correspond to the scale systematics by changing the scales by a factor of 2.

order of 130 Higgses are produced at energies $\sim\mathcal{O}(100\ \mathrm{TeV})$.

We also expect that a similar conclusion will hold for the production of the massive vector bosons (W's and Z's) in the electroweak gauge sector. In the preliminary studies in Ref. [10], it was shown that similarly to the case of massive scalars, the high-multiplicity production of the longitudinal components of the massive vector bosons also exhibits the factorial growth of the tree-level amplitudes. We plan to return to these studies in the near future.

IV. CONVOLUTION WITH PARTON DISTRIBUTION FUNCTIONS

The PDFs have a huge influence for the production of a few Higgs bosons, as can be seen in Fig. 5, where we plot the leading-order cross sections with up to four Higgs bosons computed by Madgraph5_aMC@NLO. The lower panel in this figure shows the ratio of these cross sections to the ones obtained at 8 TeV. The larger the number of Higgses produced, the bigger the enhancement with the collider energy, as expected from the PDF enhancement effect of a more energetic collider. On the other hand, the cross sections drop by a few orders of magnitude for each extra Higgs in the final state. As a matter of fact, the PDFs' rapid fall heavily suppresses the rate of processes with a higher threshold.

Although the energy of the exponential growth for the production of many Higgses is within the reach of the FCC, one could wonder if this effect is not completely washed away by PDF suppression due to the very high threshold. We show in Fig. 6 that this is not the case, and the rapid growth of partonic rates leads to picobarn cross sections already for a 50 TeV collider for the production of $\gtrsim$140 bosons. For a lower-energy collider, the PDFs are killing the cross section before reaching the fast growth regime. On the right plot of Fig. 6, we display the cross sections with a lower cut on the average kinetic energy ε per particle per mass. Since this variable is directly related to the partonic center of mass energy,

$$\sqrt{\hat{s}} = (\varepsilon + 1)nM_h, \tag{4.1}$$

this cut is equivalent to a cut on the partonic energy of the collision. It should be noted that the largest contribution to the cross section occurs when ε is $\sim$ a few (neither large nor small). Much higher values of ε are just not kinematically available. On the other side, the threshold is quite suppressed, such that the contribution of the region $\varepsilon \lesssim 1$ is also negligible. The plot only includes the contribution of the boxes, since these are expected to be dominant for large values of ε, and are of the same size as the other even polygons for $\varepsilon \sim 1$, as shown in the previous section.

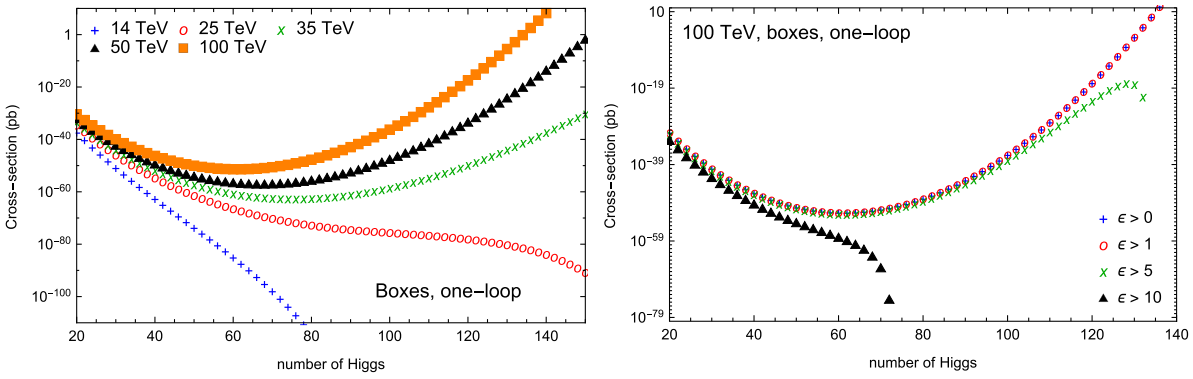

FIG. 6. Left panel: Cross sections for multi-Higgs production (3.6) at proton colliders, including the PDFs for different energies of the proton-proton collisions plotted as the function of the Higgs multiplicity. Only the contributions from the boxes are included. Right panel: The dependence on the average energy variable ε, illustrated by applying a sequence of cuts on ε at 100 TeV.

V. CONCLUSIONS

We have carried out a detailed study of multi-Higgs production processes in the gluon fusion channel in the high-energy regime relevant to future circular hadron colliders and in the high-Higgs-multiplicity limit. Our results are based on the computation of the leading polygons—the triangles, boxes, pentagons and hexagons—to the scattering processes, further combined with the subsequent branchings to reach high final-state multiplicities.

We find that the characteristic energy and multiplicity scales where these perturbative rates become observable and grow exponentially with increasing energy are within the 50 and 100 TeV regime with on the order of 130 Higgses (or more) in the final state. This is the regime where a dramatic change away from the usual weakly coupled perturbative description of the electroweak physics should occur. One can speculate that this is related to transitioning to a classicalization regime [36,37] (albeit in nongravitational QFT settings), where the dominant processes above the critical energy scale correspond to the higher and higher numbers of the relatively soft Higgs and vector bosons appearing in the final state (before their decay). It is not expected that the perturbation theory would be a valid description in this regime, but it does provide an indication for the critical values of the energy and occupation numbers.

ACKNOWLEDGMENTS

We would like to thank Gia Dvali, Cezar Gomez, Valentin Hirschi, and Joerg Jaeckel for enlightening discussions. This work is supported by STFC through the IPPP grant. O. M. and C. D. are Durham International Junior Research Fellows. The research of V. V. K. is supported in part by a Royal Society Wolfson Research Merit Award.

APPENDIX: TREE-LEVEL AMPLITUDES AT THRESHOLD

Here we will provide a brief overview of the generating functions approach for computing tree-level scattering amplitudes on multiparticle mass thresholds. This elegant formalism pioneered by Lowell Brown in Ref. [7] is based on solving classical equations of motion and bypasses the summation over individual Feynman diagrams. The overview below is included primarily for the reader's convenience; our presentation follows closely an earlier discussion of Brown's technique in Sec. II of Ref. [10].

The amplitude $\mathcal{A}_{1\to n}$ for a scalar field ϕ to produce n particles with mass M and momenta $p_1^\mu, \ldots p_n^\mu$ is found by taking the matrix element of ϕ between the vacuum states in the presence of an external source, $\rho(x)$, $\langle 0_{\rm out}|\phi(0)|0_{\rm in}\rangle_\rho$, differentiating it n times with respect to the source ρ, and applying the LSZ reduction,

$$\langle n|\phi(x)|0\rangle = \lim_{\rho\to 0}\left(\prod_{j=1}^{n}\lim_{p_j^2\to M^2}\int d^4x_j e^{ip_j\cdot x_j}(M^2-p_j^2)\frac{\delta}{\delta\rho(x_j)}\right) \times \langle 0_{\rm out}|\phi(x)|0_{\rm in}\rangle_\rho. \quad \text{(A1)}$$

The approach, of course, is general, but for concreteness we will consider first the simplest scalar ϕ^4 field theory with the Lagrangian (including the source term $\rho\phi$),

$$\mathcal{L}_\rho(\phi) = \frac{1}{2}(\partial\phi)^2 - \frac{1}{2}M^2\phi^2 - \frac{1}{4}\lambda\phi^4 + \rho\phi. \quad \text{(A2)}$$

We now make use of two simplifying conditions which will reduce dramatically the technical complexity of the problem. The first simplifying point is that we intend to sum up only the tree-level processes; hence we can work at the zeroth order in the loop expansion parameter $\bar{h}$. This is captured by the classical dynamics. Specifically, the tree-level approximation is obtained by replacing the matrix element $\langle 0_{\rm out}|\phi(x)|0_{\rm in}\rangle_\rho$ on the rhs of (A1) with a solution $\phi_{\rm cl}(\rho;x)$ to the classical field equations corresponding to the Lagrangian $\mathcal{L}_\rho(\phi)$. The presence of the source $\rho(x)$ in the Lagrangian $\mathcal{L}_\rho(\phi)$ implies that the classical field is a functional of the source and can be differentiated with respect to it, as required by (A1).

The second simplification arises from reducing the $1\to n$ kinematics to the n-particle mass threshold limit. This corresponds to making all outgoing particles to be produced at rest, $\vec{p}_j = 0$. In this limit, it is sufficient to consider the spatially independent source $\rho(t)$. Specifically, before taking the $p_j^2\to M^2$ limit in (A1), we set all outgoing momenta to $p_j^\mu = (\omega,\vec{0})$, and choose $\rho(t) = \rho_0(\omega)e^{i\omega t}$. This amounts to the second substitution on the rhs of (A1):

$$(M^2-p_j^2)\frac{\delta}{\delta\rho(x_j)}\phi_{\rm cl}(\rho;x) \to (M^2-\omega^2)\frac{\delta}{\delta\rho(t_j)}\phi_{\rm cl}(\rho;t) = \frac{\delta}{\delta z(t_j)}\phi_{\rm cl}(z;t). \quad \text{(A3)}$$

In the rightmost part of the above equation, we have absorbed the factor of $M^2-\omega^2$ into the definition of the source by writing $\rho_0(\omega) = (M^2-\omega^2)z_0(\omega)$ and defining the rescaled source variable $z(t) = z_0e^{i\omega t}$. Importantly, one can now take the required on-shell limit $\omega\to M$ simultaneously with sending $\rho_0(\omega)$ to zero such that z_0 remains finite [7]:

$$z(t) = \left(\frac{\rho_0(\omega)}{M^2-\omega^2}e^{i\omega t}\right)_{\omega\to M} \to z_0e^{iMt}. \quad \text{(A4)}$$

The resulting classical field $\phi_{\rm cl}(z(t))$, expressed as the function of the rescaled source $z(t)$, now solves the *homogeneous* classical equation, since we arranged for the source term $\rho(t)$ to vanish in our double-scaling on-shell limit $\omega\to M$, $\rho_0\to 0$.

It then follows from Eqs. (A1) and (A3) that the tree-level amplitude $\mathcal{A}_{1\to n}$ at the n-particle threshold is obtained by a simple differentiation of $\phi_{\rm cl}(z(t))$:

$$\mathcal{A}_{1\to n} = \langle n|\phi(0)|0\rangle = \left(\frac{\partial}{\partial z}\right)^n \phi_{\rm cl}\Big|_{z=0}. \tag{A5}$$

The generating function $\phi_{\rm cl}(t)$ is a solution of the ordinary differential equation without source; in the theory (A2), the equation is

$$d_t^2\phi + M^2\phi + \lambda\phi^3 = 0. \tag{A6}$$

To give the generating function of amplitudes at multi-particle thresholds, the solution must contain only the positive-frequency components of the form $e^{+{\rm i}nMt}$, where n is the number of final-state particles in the amplitude $\mathcal{A}_{1\to n}$. This follows immediately from (A5). Thus, the solution we are after is given by the Taylor expansion in powers of the complex variable $z(t)$,

$$\phi_{\rm cl}(t) = \sum_{n=1}^{\infty} a_n z(t)^n. \tag{A7}$$

In the limit where interactions are switched off, $\lambda = 0$, the correctly normalized solution is $\phi_{\rm cl} = z(t)$, and this fixes the first coefficient $a_1 = 1$ on the rhs of (A7). As the solution contains only positive-frequency harmonics, it is a complex function of Minkowski time. This also fixes the initial conditions of the solution, $\phi_{\rm cl}(t) \to 0$, as ${\rm Im}(t) \to \infty$. In Euclidean time, the solution is real.

The Taylor expansion coefficients a_n in (A7) determine the actual amplitudes via (A5) giving $\mathcal{A}_{1\to n} = n!a_n$. The classical generating function approach of Ref. [7] amounts to finding the $\vec{x}$-independent solution of the Euler-Lagrange equations as an analytic function of z in the form (A7), and computing the amplitudes via (A5).

The classical generating function for the theory defined by (A2) is surprisingly simple and can be written in closed form [7]:

$$\phi_{\rm cl}(t) = \frac{z(t)}{1 - \frac{\lambda}{8M^2} z(t)^2}. \tag{A8}$$

It is easily checked that the expression in (A8) solves the classical equation (A6) and has the correct form, $\phi_{\rm cl} = z + \ldots$ as $z \to 0$. The corresponding tree-level amplitudes on mass thresholds in the theory (A2) are then given by

$$\mathcal{A}_{1\to n} = \left(\frac{\partial}{\partial z}\right)^n \phi_{\rm cl}\Big|_{z=0} = n!\left(\frac{\lambda}{8M^2}\right)^{\frac{n-1}{2}} \tag{A9}$$

and exhibit factorial growth with the number of particles n in the external state.

This general approach is also readily applied to the theory (1.2) with the nonvanishing VEV relevant to the high-multiplicity Higgs production studied in the present paper. In this case, the classical equation is given by Eq. (1.5), and one searches for the particular solution in the form $h_{\rm cl} = v + z + \mathcal{O}(z^2)$, where the z^0 term is the VEV. Instead of solving the second-order ordinary differential equation (1.5), one can consider an equivalent problem which results from computing the first integral of motion of the Euclidean problem associated with the theory (1.2). In this case, one considers the first integral of motion—the energy E—in Euclidean time. E must be constant on the classical trajectory, and in the case at hand, $E = 0$,

$$E := \int dt\left(\frac{1}{2}(d_\tau h)^2 - \frac{\lambda}{4}(h^2 - v^2)^2\right) = 0, \tag{A10}$$

where $d_\tau h$ denotes the derivative of the field with respect to the imaginary time $\tau = it$. This amounts to solving the first-order differential equation

$$d_\tau h = \sqrt{\lambda/2}(h^2 - v^2), \tag{A11}$$

or in Minkowski time,

$$-{\rm i}d_t h = \sqrt{\lambda/2}(h^2 - v^2). \tag{A12}$$

The general solution of the first-order differential equation easily found by the separation of variables, and, in particular, the imaginary-time equation (A11), is solved by the hyperbolic tangent. Its analytic continuation to real time is

$$h_{\rm cl}(t) = v\frac{1 + \frac{z(t)}{2v}}{1 - \frac{z(t)}{2v}}, \quad \text{where } z = z_0 e^{{\rm i}\sqrt{2\lambda}vt}. \tag{A13}$$

This is precisely the Brown's solution (1.6) used in the body of the paper, and it can also be checked by direct substitution that the expression (A13) solves both the original classical second-order differential equation (1.5) and the first-order equation (A12). Taylor-expanding (A13) in z gives

$$h_{\rm cl}(t) = v + 2v\sum_{n=1}^{\infty}\left(\frac{z(t)}{2v}\right)^n, \tag{A14}$$

which has the z correct boundary conditions $h_{\rm cl} = v + z + \mathcal{O}(z^2)$ at $z \to 0$.

[1] J. M. Cornwall, On the high-energy behavior of weakly coupled gauge theories, Phys. Lett. B **243**, 271 (1990).

[2] H. Goldberg, Breakdown of perturbation theory at tree level in theories with scalars, Phys. Lett. B **246**, 445 (1990).

[3] M. B. Voloshin, Estimate of the onset of nonperturbative particle production at high-energy in a scalar theory, Phys. Lett. B **293**, 389 (1992).

[4] J. Jaeckel and V. V. Khoze, Upper limit on the scale of new physics phenomena from rising cross sections in high multiplicity Higgs and vector boson events, Phys. Rev. D **91**, 093007 (2015).

[5] V. V. Khoze, Diagrammatic computation of multi-Higgs processes at very high energies: Scaling $\log \sigma_n$ with MadGraph, Phys. Rev. D **92**, 014021 (2015).

[6] B. W. Lee, C. Quigg, and H. B. Thacker, The Strength of Weak Interactions at Very High-Energies and the Higgs Boson Mass, Phys. Rev. Lett. **38**, 883 (1977); Weak interactions at very high-energies: The role of the Higgs boson mass, Phys. Rev. D **16**, 1519 (1977).

[7] L. S. Brown, Summing tree graphs at threshold, Phys. Rev. D **46**, R4125 (1992).

[8] E. N. Argyres, R. H. P. Kleiss, and C. G. Papadopoulos, Amplitude estimates for multi-Higgs production at high-energies, Nucl. Phys. **B391**, 42 (1993).

[9] M. V. Libanov, V. A. Rubakov, D. T. Son, and S. V. Troitsky, Exponentiation of multiparticle amplitudes in scalar theories, Phys. Rev. D **50**, 7553 (1994).

[10] V. V. Khoze, Multiparticle Higgs and vector boson amplitudes at threshold, J. High Energy Phys. 07 (2014) 008.

[11] E. N. Argyres, R. H. P. Kleiss, and C. G. Papadopoulos, Perturbative unitarity constraints on scalar self-interactions, Phys. Lett. B **296**, 139 (1992).

[12] M. B. Voloshin, Summing one loop graphs at multiparticle threshold, Phys. Rev. D **47**, R357 (1993).

[13] B. H. Smith, Summing one loop graphs in a theory with broken symmetry, Phys. Rev. D **47**, 3518 (1993).

[14] E. N. Argyres, C. G. Papadopoulos, and R. H. P. Kleiss, Multiscalar production amplitudes beyond threshold, Nucl. Phys. **B395**, 3 (1993).

[15] Y. Makeenko, Exact multiparticle amplitudes at threshold in large N component ϕ^4 theory, Phys. Rev. D **50**, 4137 (1994).

[16] M. V. Libanov, Multiparticle threshold amplitudes exponentiate in arbitrary scalar theories, Mod. Phys. Lett. A **11**, 2539 (1996).

[17] D. T. Son, Semiclassical approach for multiparticle production in scalar theories, Nucl. Phys. **B477**, 378 (1996).

[18] F. L. Bezrukov, M. V. Libanov, D. T. Son, and S. V. Troitsky, Singular classical solutions and tree multiparticle cross-sections in scalar theories, arXiv:hep-ph/9512342.

[19] F. L. Bezrukov, Use of singular classical solutions for calculation of multiparticle cross-sections in field theory, Teor. Mat. Fiz. **115**, 358 (1998) [Theor. Math. Phys. **115**, 647 (1998)].

[20] M. V. Libanov, V. A. Rubakov, and S. V. Troitsky, Multiparticle processes and semiclassical analysis in bosonic field theories, Phys. Part. Nucl. **28**, 217 (1997).

[21] M. V. Libanov, D. T. Son, and S. V. Troitsky, Exponentiation of multiparticle amplitudes in scalar theories: 2. Universality of the exponent, Phys. Rev. D **52**, 3679 (1995).

[22] V. V. Khoze, Perturbative growth of high-multiplicity W, Z and Higgs production processes at high energies, J. High Energy Phys. 03 (2015) 038.

[23] J. Alwall, M. Herquet, F. Maltoni, O. Mattelaer, and T. Stelzer, MadGraph 5: Going beyond, J. High Energy Phys. 06 (2011) 128.

[24] J. Alwall, R. Frederix, S. Frixione, V. Hirschi, F. Maltoni, O. Mattelaer, H.-S. Shao, T. Stelzer, P. Torrielli, and M. Zaro, The automated computation of tree-level and next-to-leading order differential cross sections, and their matching to parton shower simulations, J. High Energy Phys. 07 (2014) 079.

[25] E. W. N. Glover and J. J. van der Bij, Higgs boson pair production via gluon fusion, Nucl. Phys. **B309**, 282 (1988).

[26] T. Plehn, M. Spira, and P. M. Zerwas, Pair production of neutral Higgs particles in gluon-gluon collisions, Nucl. Phys. **B479**, 46 (1996); **B531**, 655(E) (1998).

[27] T. Binoth, S. Karg, N. Kauer, and R. Ruckl, Multi-Higgs boson production in the Standard Model and beyond, Phys. Rev. D **74**, 113008 (2006).

[28] S. Borowka, N. Greiner, G. Heinrich, S. P. Jones, M. Kerner, J. Schlenk, U. Schubert, and T. Zirke, Higgs Boson Pair Production in Gluon Fusion at NLO with Full Top-Quark Mass Dependence, Phys. Rev. Lett. **117**, 012001 (2016); **117**, 079901(E) (2016).

[29] A. Papaefstathiou and K. Sakurai, Triple Higgs boson production at a 100 TeV proton-proton collider, J. High Energy Phys. 02 (2016) 006.

[30] B. Fuks, J. H. Kim, and S. J. Lee, Probing Higgs self-interactions in proton-proton collisions at a center-of-mass energy of 100 TeV, Phys. Rev. D **93**, 035026 (2016).

[31] J. Baglio, A. Djouadi, and J. Quevillon, Prospects for Higgs physics at energies up to 100 TeV, Rep. Prog. Phys. **79**, 116201 (2016).

[32] C. Y. Chen, Q. S. Yan, X. Zhao, Y. M. Zhong, and Z. Zhao, Probing triple-Higgs productions via $4b2\gamma$ decay channel at a 100 TeV hadron collider, Phys. Rev. D **93**, 013007 (2016).

[33] V. Hirschi and O. Mattelaer, Automated event generation for loop-induced processes, J. High Energy Phys. 10 (2015) 146.

[34] A. Alloul, N. D. Christensen, C. Degrande, C. Duhr, and B. Fuks, FeynRules 2.0: A complete toolbox for tree-level phenomenology, Comput. Phys. Commun. **185**, 2250 (2014).

[35] A. D. Martin, W. J. Stirling, R. S. Thorne, and G. Watt, Parton distributions for the LHC, Eur. Phys. J. C **63**, 189 (2009).

[36] G. Dvali, G. F. Giudice, C. Gomez, and A. Kehagias, UV-completion by classicalization, J. High Energy Phys. 08 (2011) 108.

[37] G. Dvali, D. Flassig, C. Gomez, A. Pritzel, and N. Wintergerst, Scrambling in the black hole portrait, Phys. Rev. D **88**, 124041 (2013).